J Clust Sci (2017) 28:1393–1405
DOI 10.1007/s10876-016-1155-z

ORIGINAL PAPER

# Theoretical Investigation of Electronic Properties of Undoped and Ag-Doped $(CdTe)_{16\times N}$ Multi-cage Nanochains

**Fengyi Suo**[1] · **Yonghong Zhang**[1] · **Shiping Huang**[2]

Received: 17 July 2016 / Published online: 28 December 2016

**Abstract** The structural and electronic properties of highly stable structures, undoped and Ag substitutional doped $(CdTe)_{16\times N}$ ($N = 1$–3) multi-cage nanochains, have been investigated by density functional theory. $(CdTe)_{16}$ cage is chosen as the building unit to form $(CdTe)_{16\times N}$ multi-cage nanochains. Two possible assembly modes, interconnecting two cages by their four-membered rings and interconnecting two cages by their six-membered rings, are considered. For Ag doping, two different substitutional sites have been studied. Our results show that the multi-cage nanochains have higher stability than that of the single cage, and the stability varies with the assembly modes and doping sites for both undoped and Ag-doped nanochains. After Ag doping, an acceptor level is observed, showing typical *p*-type properties. The properties of energy structure, charge density and density of states are analyzed in detail. Results show that the assembly modes and Ag substitutional doping site have a significant impact on the electronic properties of Ag-doped $(CdTe)_{16\times N}$ multi-cage nanochains.

**Keywords** Cadmium telluride · Multi-cage nanochain · Substitutional doping · Density functional theory

## Introduction

II–VI semiconductor material, CdTe nanocluster, is one of the most promising optoelectronic materials due to its optimum band gap, high optical absorption coefficient. The tunability of the electronic properties of CdTe nanocluster by

---

✉ Yonghong Zhang
zhangyonghong@tjpu.edu.cn

[1] Department of Physics, Tianjin Polytechnic University, Tianjin 300387, People's Republic of China

[2] State Key Laboratory of Organic-Inorganic Composites, Beijing University of Chemical Technology, Beijing 100029, People's Republic of China

adjusting its size to change quantum confinement and doping with metal atoms makes it quite significant in nano-devices [1, 2]. Different CdTe quantum dots have been synthesized experimentally and used in various sorts of optoelectronic devices, such as solar cells, optical detectors, and light emitting diodes [3–6]. However, deep understanding of the relationships between structures and electronic properties experimentally is still a challenge. To investigate properties of CdTe nanoclusters, many possible $Cd_nTe_n$ structures have been proposed and studied by first principles calculations [7–12]. Two families of structures, endohedral (or core–shell) cage structures and hollow cage structures of $Cd_nTe_n$ ($n < 30$) are reported. The electronic properties show to be influenced by their structures [7–9].

Furthermore, doped nanoclusters have attracted great attention due to the modification of properties by doping with different atoms. Substitutional doping is a process in which atoms are intentionally used to replace some atoms of the initial structure to alter its properties [13, 14]. To change the optical and electronic properties, some doped II–VI semiconductor nanoclusters doped with metals, such as Ag, Cu, Pb, In, were studied both experimentally and theoretically [15–17]. The *p*-type and *n*-type semiconductors were obtained by substitutional doping CdTe nanoclusters with Pd, Ag, In, and Sn respectively [1]. The metal-doped nanoclusters were found to be more stable than the undoped nanoclusters. The same result was observed in Ag-doped ZnSe by density functional theory [16]. The HOMO–LUMO gap was also observed to change to a great extent according to different doping atoms.

Based on the importance of metal-doped CdTe nanoclusters and reported research results, we investigated the structural and electronic properties of pure $(CdTe)_{16\times N}$ multi-cage nanochains ($N = 1$–$3$) and Ag-doped $(CdTe)_{16\times N}$ multi-cage nanochains ($N = 1, 2$) in this paper. $(CdTe)_{16}$ cage was chosen as the building unit to form multi-cage nanochains. Two possible modes of forming multi-cage nanochains were studied. The electronic properties including binding energy, energy gap, the density of states, the charge densities of the highest occupied molecular orbital (HOMO) and the lowest unoccupied molecular orbital (LUMO) were analyzed. Then, a Cd atom was substituted by Ag atom in $(CdTe)_{16\times N}$ multi-cage nanochains ($N = 1, 2$). Two possible substitutional sites, site I and site II, were considered. By comparing the structural and electronic properties of undoped and doped $(CdTe)_{16\times N}$ nanoclusters, we found that the stability of these nanoclusters is promoted by Ag doping, and the electronic properties are affected by substitutional doping atom sites and assembly modes.

## Computational Method

The $(CdTe)_{16\times N}$ ($N = 1$–$3$) multi-cage nanochains and Ag-doped $(CdTe)_{16\times N}$ ($N = 1, 2$) multi-cage nanochains have been studied by the well-known density functional theory (DFT) [18–20] implemented in the DMol3 package within the framework of generalized-gradient approximation (GGA) with the Perdew, Burke, and Ernzerhof exchange–correlation functional (PBE) [21, 22]. The geometries of all undoped and doped $(CdTe)_{16\times N}$ nanoclusters were optimized without symmetry constraints. The convergence tolerance was set to be $10^{-5}$ Ha for energy. For Ag-doped $(CdTe)_{16\times N}$ ($N = 1, 2$) multi-cage nanochains, the spin-polarized calculation was performed. The atomic orbital basis set, double numerical plus polarization (DNP) [20, 21], was employed in the calculation with 4.6 Å global orbital cutoff. The total energy convergence criterion used for electronic self-consistency (SCF) was $1.0 \times 10^{-6}$ Ha. The smearing of 0.005 Ha was used for these systems to accelerate SCF convergence. The vibration frequency option was carried out in order to verify the stabilities of structures.

The stabilities of single cages $(CdTe)_n$ were analyzed. Due to the higher stability and symmetry, $(CdTe)_{16}$ cage was selected as the basic unit to form multi-cage nanochains. Two possible assembly modes, interconnecting two $(CdTe)_{16}$ cages by their four-membered rings and interconnecting two $(CdTe)_{16}$ cages by their six-membered rings with the number of cages $N = 1$–3, were taken into account. Thus, two kinds of multi-cage nanochains were obtained. For Ag substitutional doping nanoclusters, a Cd atom of a nanocluster was substituted by an Ag atom. Two different substitutional sites, Cd atom shared by two six-membered rings and one four-membered ring (site I) and Cd atom shared by three six-membered rings (site II), were considered respectively. The geometries of the undoped and doped nanoclusters were optimized. In geometry optimization, structures relaxed to minimize their total energy to reach the stable structures.

In order to get the electronic densities of states (DOS) of undoped and doped $(CdTe)_{16\times N}$ nanoclusters and avoid any spurious inter-cluster interactions, a large orthorhombic supercell and its periodic images were used. The nanocluster was placed at the center of the supercell. The distance from the surface of the nanocluster to the simulation supercell boundary was larger than 20 Å. The DOS and PDOS were calculated in the periodic boundary conditions.

## Results and Discussions

### The Structural and Electronic Properties of $(CdTe)_{16\times N}$ Multi-cage Nanochains

The basic unit $(CdTe)_{16}$ cage is composed of six four-membered rings and twelve six-membered rings with $T_d$ symmetry as shown in Fig. 1. Based on its geometry structure, the two kinds of nanoclusters, IFMR and ISMR nanochains, were built. After geometry optimization, these $(CdTe)_{16\times N}$ nanochains relaxed to reach their most stable structures as shown in Fig. 1. In these structures, no matter which mode, IFMR or ISMR, the two cages are connected by four bonds even for ISMR mode. Besides, the $T_d$ symmetry of single $(CdTe)_{16}$ cage changes to $D_{2d}$ for $(CdTe)_{16\times N}$ IFMR nanochains and $C_{2h}$, $C_{2v}$ for $(CdTe)_{16\times N}$ ISMR nanochains.

To investigate the stabilities of the $(CdTe)_{16\times N}$ nanochains, the binding energy $E_b$ of per Cd–Te unit was calculated by using the following equation,

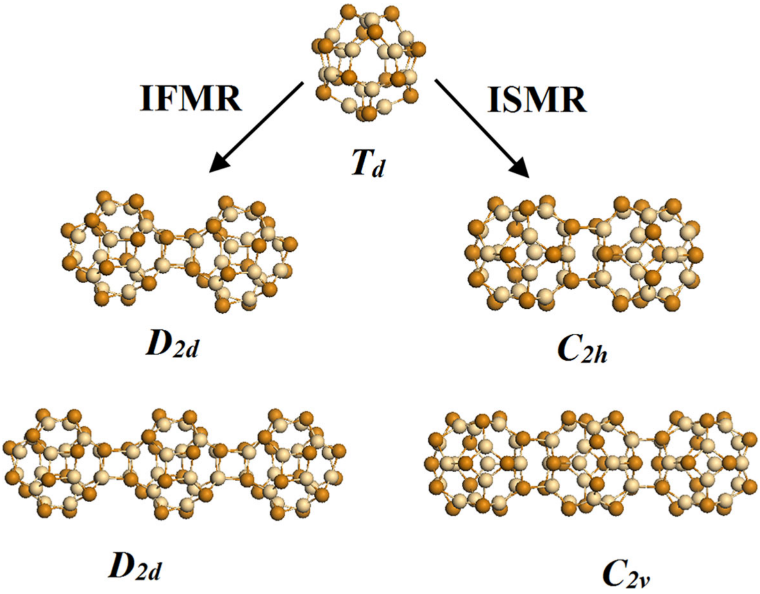

**Fig. 1** The geometries of $(CdTe)_{16\times N}$ ($N = 1$–3) IFMR and ISMR multi-cage nanochains with corresponding point group symmetry. *Dark brown* and *light brown balls* represent Te and Cd atoms respectively (Color figure online)

$$E_b = \{N \times [16 \times E(\mathrm{Cd}) + 16 \times E(\mathrm{Te})] - E((\mathrm{CdTe})_{16\times N})\}/(16 \times N)$$

where $E(\mathrm{Cd})$, $E(\mathrm{Te})$ and $E((\mathrm{CdTe})_{16\times N})$ represent the total energies of individual Cd, Te atoms and $(CdTe)_{16\times N}$ nanochains respectively. The average binding energies of per Cd–Te unit of $(CdTe)_{16\times N}$ nanochains are listed in Table 1. As we can see, with the increase of $N$, the binding energy $E_b$ changes from 3.638 eV (single cage) to 3.655 eV [$(CdTe)_{16\times 3}$ IFMR nanochains] and 3.652 eV [$(CdTe)_{16\times 3}$ ISMR nanochains], which shows that the binding energy increases with the growth of $N$. The $(CdTe)_{16\times N}$ multi-cage nanochains are more stable than the single cage, which is the same as the former studied $(CdTe)_{12\times N}$ nanoclusters [9]. However, contrary to earlier studied $(CdTe)_{12\times N}$ nanoclusters [9], the $(CdTe)_{16\times N}$

**Table 1** The binding energy $E_b$ of per Cd–Te unit, HOMO–LUMO energy gap $E_g$, and the size $L$ of $(CdTe)_{16\times N}$ nanochains ($N = 1$–3)

| Cluster | Structure | $E_b$ (eV/unit) | $E_g$ (eV) | $L$ (nm) |
|---|---|---|---|---|
| $(CdTe)_{16\times 1}$ | Single cage | 3.638 | 2.36 | 1.04 |
| $(CdTe)_{16\times 2}$ | IFMR | 3.651 | 2.14 | 2.24 |
| | ISMR | 3.649 | 2.07 | 2.16 |
| $(CdTe)_{16\times 3}$ | IFMR | 3.655 | 2.08 | 3.47 |
| | ISMR | 3.652 | 2.02 | 3.27 |

IFMR nanochains show to have higher stability than the ISMR nanochains with the same *N*.

The energy gaps of $(CdTe)_{16\times N}$ nanochains, the energy differences of the highest occupied molecular orbital and the lowest unoccupied molecular orbital (HOMO–LUMO), were also calculated and shown in Table 1. From the Table 1, we can find that the energy gaps decrease with *N* increase, from 2.36 to 2.08 eV for IFMR nanochains and 2.02 eV for ISMR nanochains. Since size increases with *N*, the energy gaps of $(CdTe)_{16\times N}$ nanochains exhibit to decrease with the increase of the nanocluster size, showing typical quantum dot character [23]. Furthermore, the $(CdTe)_{16\times N}$ ISMR nanochains have the narrower energy gap comparing to the IFMR nanochains with the same *N*, which is the same as $(CdTe)_{12\times N}$ nanochains [9]. More energy is needed to excite electrons from the highest occupied valence band to the lowest unoccupied conduction band for $(CdTe)_{16\times N}$ IFMR nanochains.

In order to understand the energy structure, the total and partial densities of states of $(CdTe)_{16\times N}$ nanochains are investigated. Similar results are observed for both IFMR and ISMR nanochains. Here, only the DOS and PDOS of $(CdTe)_{16\times N}$ IFMR nanochains are shown in Fig. 2, in which the Fermi level is shifted to 0 eV and plotted in dotted line. Figure 2 shows that the energy band is divided into two parts: the lower energy band with energy from −12.27 to 0 eV and the higher energy band with energy from 1.98 to 3.30 eV. The energy difference between the lower energy band and the higher energy band is observed to decrease with *N* increase, which is consistent with the analysis of HOMO–LUMO energy gap. From the PDOS, the contributions to the top of the valence band are observed mainly from *p*-orbital with minor *d*-orbital, which is in good agreement with the valence configurations of Cd ($4d^{10}5s^2$) and Te ($5s^25p^4$).

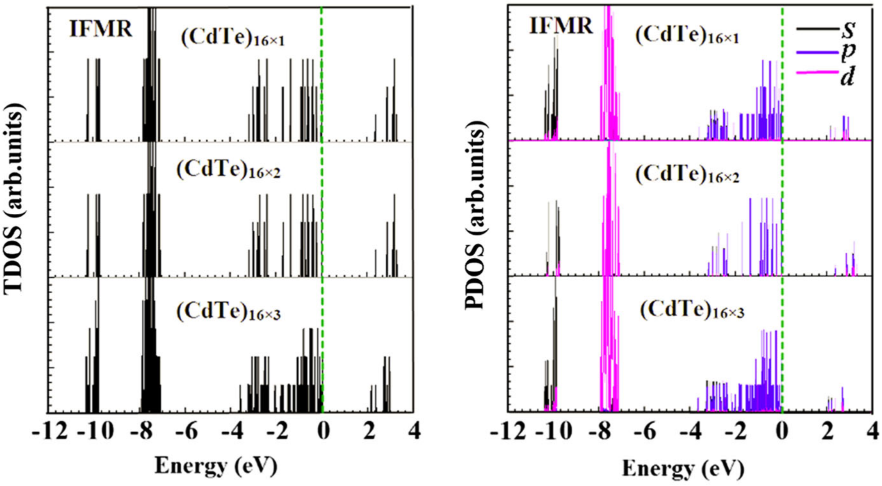

**Fig. 2** The total (TDOS) and partial densities of states (PDOS) of $(CdTe)_{16\times N}$ IFMR nanochains. The Fermi level is shifted to 0 eV

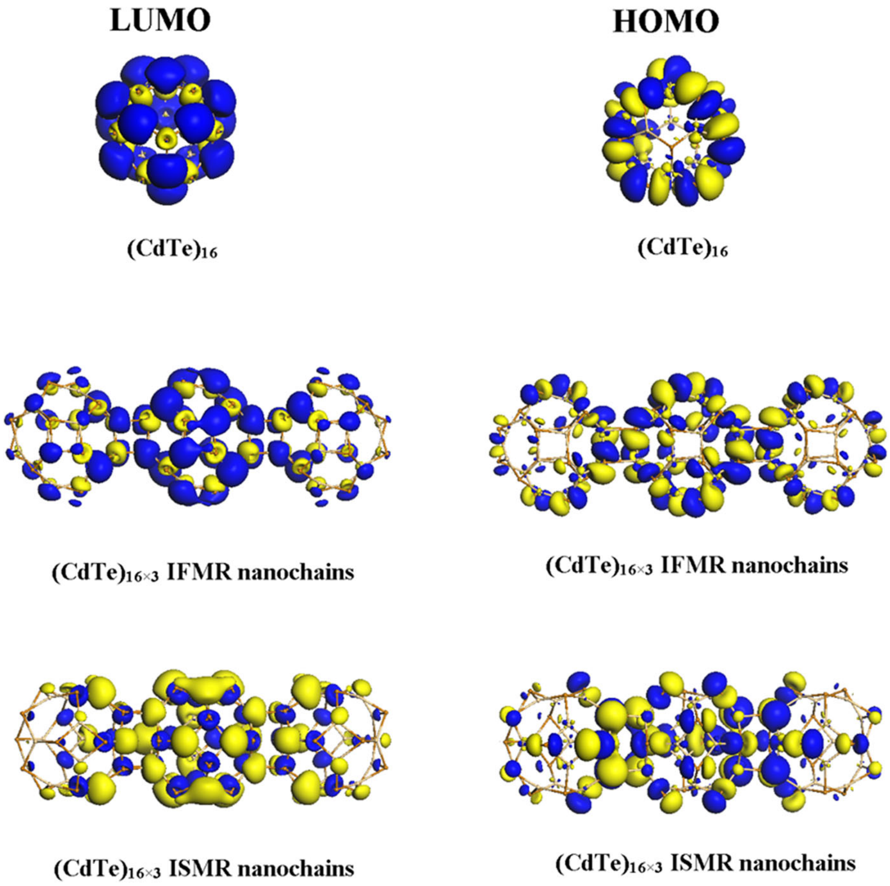

**Fig. 3** The charge densities of the LUMO and HOMO of $(\mathrm{CdTe})_{16\times N}$ nanochains ($N = 1, 3$). The *dark brown* and *light brown balls* represent Te and Cd atoms respectively (Color figure online)

To further understand the properties, the charge densities of LUMO and HOMO of $(\mathrm{CdTe})_{16\times N}$ nanochains are analyzed and plotted in Fig. 3. Also, similar behaviors are observed for both ISMR and IFMR nanochains. The LUMO is composed of Cd *s*-orbital and Te $sp^3$ hybrid orbital, while the HOMO consists of major Te *p*-orbital and Cd *d*-orbital as reported results [9], which are also consistent with PDOS analysis and Cd, Te valence configurations. Furthermore, the charge densities of LUMO and HOMO are mainly dominated by the middle cage of the nanochains, which displays different behaviors from $(\mathrm{CdTe})_{12\times N}$ nanochains [9]. The structure of basic composition unit, single cage, has great influence on the properties of nanochains.

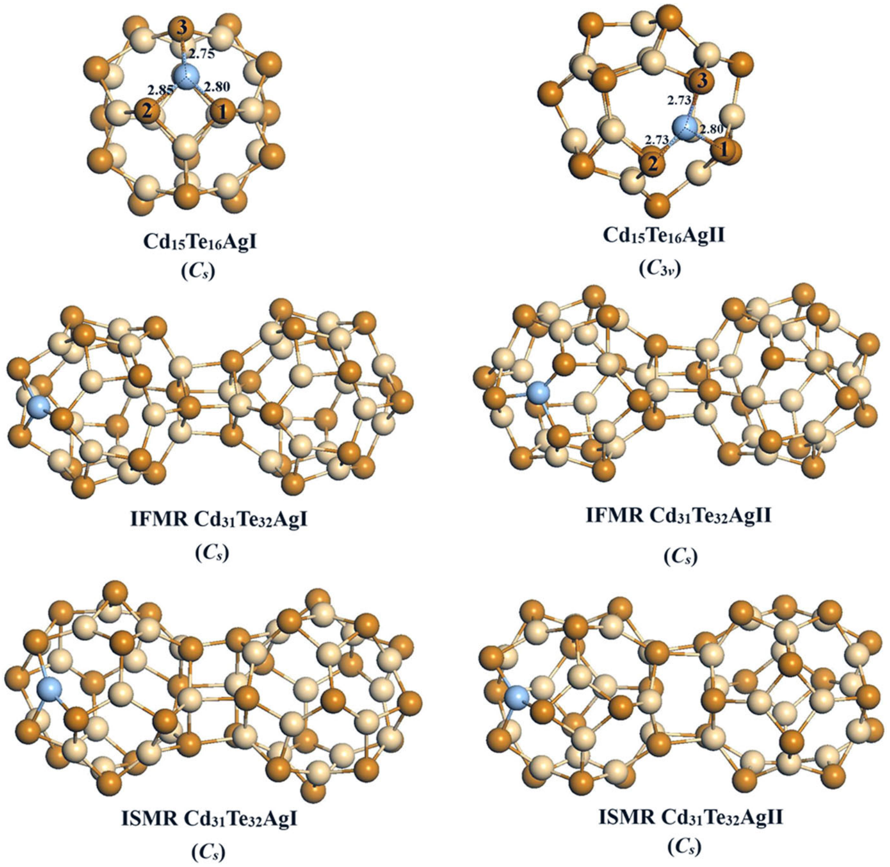

$Cd_{15}Te_{16}AgI$ ($C_s$)

$Cd_{15}Te_{16}AgII$ ($C_{3v}$)

IFMR $Cd_{31}Te_{32}AgI$ ($C_s$)

IFMR $Cd_{31}Te_{32}AgII$ ($C_s$)

ISMR $Cd_{31}Te_{32}AgI$ ($C_s$)

ISMR $Cd_{31}Te_{32}AgII$ ($C_s$)

**Fig. 4** The geometries of $Cd_{15}Te_{16}Ag$ and $Cd_{31}Te_{32}Ag$ nanoclusters with corresponding point group symmetry. The *dark brown*, *light brown* and *blue balls* represent Te, Cd, and Ag atoms respectively. I, II represent Ag doping site, site I and site II (Color figure online)

## The Structural and Electronic Properties of Ag-Doped $(CdTe)_{16\times N}$ Multi-cage Nanochains

$(CdTe)_{16}$ and $(CdTe)_{16\times 2}$ nanochains doped substitutionally with Ag atom are investigated. Only a Cd atom is substituted by an Ag atom in a nanochain. Two doping sites, Cd atom shared by two six-membered rings (site I) and one four-membered ring and Cd atom shared by three six-membered rings (site II), are considered respectively. The optimized structures are shown in Fig. 4. $Cd_{15}Te_{16}$ AgI, $Cd_{15}Te_{16}$AgII, $Cd_{31}Te_{32}$AgI, $Cd_{31}Te_{32}$AgII are used to represent doped $Cd_{15}Te_{16}Ag$ and $Cd_{31}Te_{32}Ag$ with Ag atom at site I and site II respectively. After doping, the nanoclusters relax to their lowest energy structures, which leads the $T_d$ symmetry of $(CdTe)_{16}$ to change to $Cs$ of $Cd_{15}Te_{16}$AgI and $C_{3v}$ of $Cd_{15}Te_{16}$AgII from $T_d$ of $(CdTe)_{16}$. Also, for the two cage nanochains, the initial $D_{2d}$ symmetry of

**Table 2** The binding energy $E_b$, energy band gap $E_g$ and size $L$ of undoped and Ag-doped $(CdTe)_{16\times N}$ clusters ($N = 1, 2$)

| Cluster | Structure | $E_b$ (eV) | $E_g$ (eV) | $L$ (nm) |
|---|---|---|---|---|
| $Cd_{16}Te_{16}$ | Single | 58.21 | 2.36 | 1.04 |
| $Cd_{15}Te_{16}$ AgI | Single | 58.97 | 2.36 | 1.04 |
| $Cd_{15}Te_{16}$ AgII | Single | 58.88 | 2.28 | 1.04 |
| $Cd_{32}Te_{32}$ | IFMR | 116.83 | 2.14 | 2.24 |
| $Cd_{31}Te_{32}$AgI | IFMR | 117.59 | 2.06 | 2.24 |
| $Cd_{31}Te_{32}$AgII | IFMR | 117.49 | 1.99 | 2.26 |
| $Cd_{32}Te_{32}$ | ISMR | 116.78 | 2.07 | 2.16 |
| $Cd_{31}Te_{32}$AgI | ISMR | 117.55 | 2.05 | 2.16 |
| $Cd_{31}Te_{32}$AgII | ISMR | 117.45 | 2.00 | 2.17 |

$(CdTe)_{16\times 2}$ IFMR nanochain and $C_{2h}$ symmetry of $(CdTe)_{16\times 2}$ ISMR nanochain are lost with doping.

The stabilities of Ag-doped CdTe nanoclusters are studied. The binding energy of Ag-doped $(CdTe)_{16\times N}$ nanoclusters ($N = 1, 2$) was calculated by using the following equation,

$$\begin{aligned} \boldsymbol{E_b} = {} & [(16 \times \boldsymbol{N}-1) \times \boldsymbol{E}(\mathrm{Cd}) + 16 \times \boldsymbol{N} \times \boldsymbol{E}(\mathrm{Te}) + \boldsymbol{E}(\mathrm{Ag})] \\ & - \boldsymbol{E}(\mathrm{Cd}_{16\times \boldsymbol{N}-1}\mathrm{Te}_{16\times \boldsymbol{N}}\mathrm{Ag}) \end{aligned}$$

The calculated binding energies are shown in Table 2. As we can see, the binding energy of $Cd_{15}Te_{16}$AgI and $Cd_{15}Te_{16}$AgII are 58.97 and 58.88 eV respectively, which are 0.76 and 0.67 eV higher than undoped $(CdTe)_{16}$ single cage. Also, the binding energies of Ag-doped $(CdTe)_{16\times 2}$ nanochains are larger than the corresponding undoped $(CdTe)_{16\times 2}$ nanochains, showing that the Ag-doped $(CdTe)_{16\times N}$ clusters are more stable than undoped $(CdTe)_{16\times N}$ clusters. It further proves that doping improves the stability of II–VI semiconductor nanocrytals as reported [16]. Furthermore, the doped nanoclusters with Ag at site I show to have higher stability than that with Ag at site II. Site I is the favorite doping site. IFMR nanochains are observed to be more stable than ISMR nanochains for both doped and undoped nanochains.

The DOS and PDOS of doped nanoclusters are studied and displayed in Fig. 5. In the figure, the Fermi level is shifted to 0 eV and shown in dotted line. The two bands, the lower occupied energy states (valence band) in the range of −12.56 to 0.00 eV and the higher unoccupied energy states (conduction band) in the range of 1.98–3.20 eV are observed. The energy gap, the energy difference between the top of the valence band and the bottom of the conduction band is shown in Table 2. Comparing the DOS of undoped and doped nanoclusters, the energy gaps show to decrease from original 2.36, 2.14, 2.07 to 2.28, 1.99, and 2.00 eV respectively after doping. Doping narrows the forbidden energy gap. In addition, doping site also has an influence on the energy gap. As we can observe, the energy gap is wider for Ag at site I. However, the assembly mode, IFMR and ISMR of doped two-cage nanochains, does not show any obvious effect on the energy bandgap, which presents different features from undoped nanoclusters. Besides, an obvious

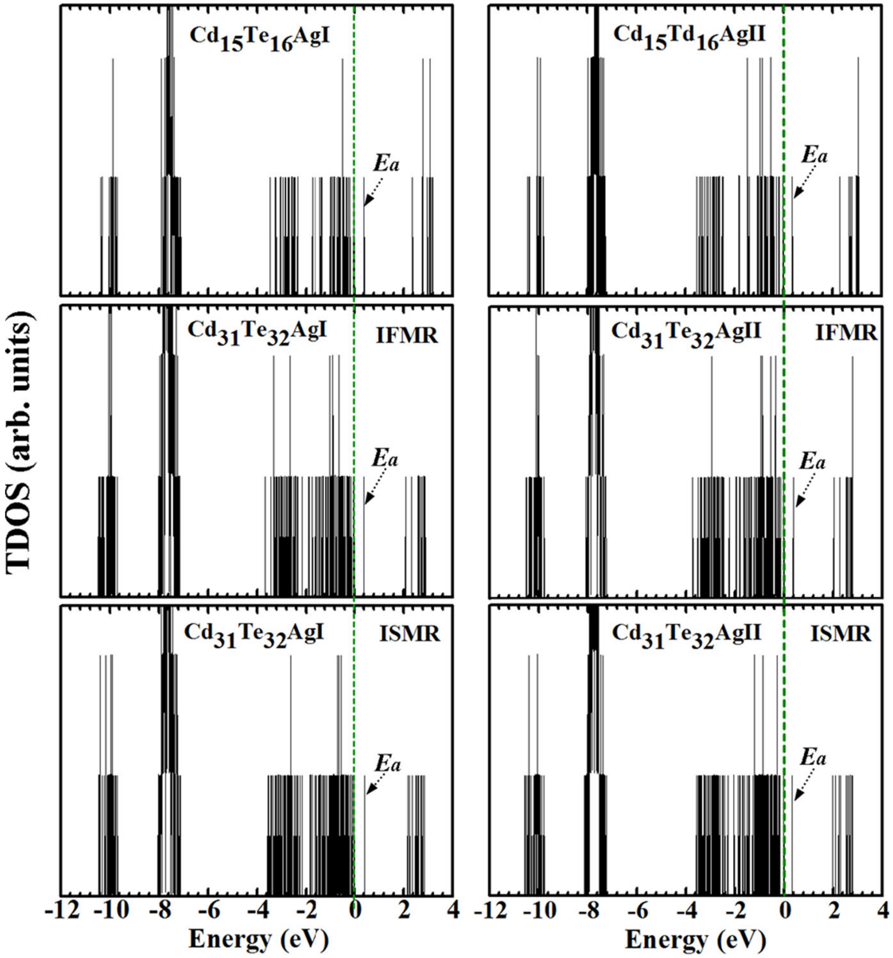

**Fig. 5** The total densities of states (TDOS) of $Cd_{15}Te_{16}Ag$ and $Cd_{31}Te_{32}Ag$ nanoclusters. The Fermi level is shifted to 0 eV

difference, a new energy level $E_a$ between the valence band and conduction band is introduced after Ag doping as shown in Fig. 5. The introduced level is lower than the middle of the energy band gap. Comparing Ag-doped single cage and two cage nanochains, the position of the introduced level moves towards the middle of the energy band gap with the number of cages. As we know, the doping concentration of single cage is higher than that of the two-cage nanochains due to different cluster size. So, the position of $E_a$ changes with doping concentration, showing typical characters of acceptor level, which is consistent with reported Ag-doped CdTe nanoclusters [1].

To fully understand the state $E_a$, the contributions of different orbital components to the densities of states are analyzed. The PDOS of *s*, *p*, *d* orbitals of Ag and its

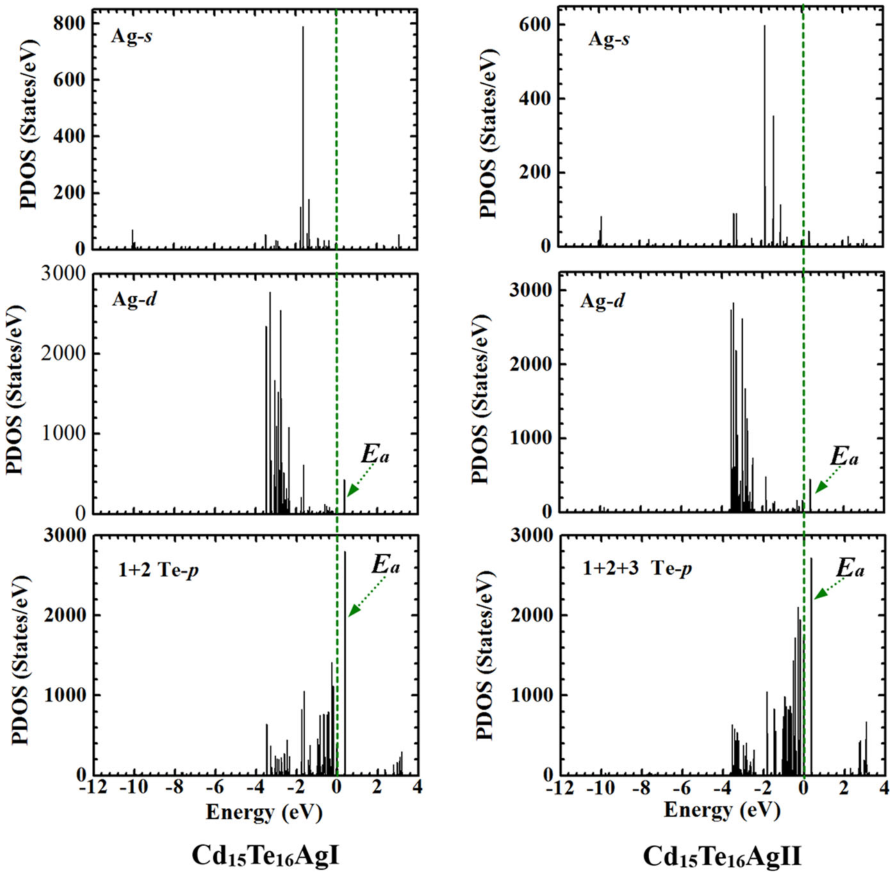

**Fig. 6** The partial densities of states (PDOS) of Ag-doped $Cd_{15}Te_{16}Ag$ nanoclusters. The Fermi level is shifted to 0 eV

neighbor Te atoms (numbered in Fig. 4) of $Cd_{15}Te_{16}AgI$ and $Cd_{15}Te_{16}AgII$ nanoclusters are plotted and shown in Fig. 6. As shown in the figure, strong Te-*p* orbital peak and weak Ag-*d* orbital peak at energy $E_a$ are observed for both nanoclusters, which indicates that the contributions to $E_a$ state are from Ag and its neighbor Te atom showing acceptor level characters. The similar results are observed for $Cd_{31}Te_{32}Ag$ two-cage nanochains.

Furthermore, the charge densities of the HOMO orbitals of Ag-doped nanoclusters are studied and plotted in Fig. 7. The HOMO corresponding to the $E_a$ state exhibits to be dominated by Ag-*d* orbital and its neighbor Te-*p* orbital for both single and two-cage nanochains, which is in good agreement with the PDOSs shown in Fig. 6. The orbital of HOMO-2 is mainly dominated by Te-*p*, Cd-*d* orbitals respectively, which is consistent with the HOMO of corresponding undoped nanoclusters. The LUMO is mainly composed of Cd *s*-orbital and Te-$sp^3$ hybrid orbital which is also consistent with the LUMO of corresponding undoped nanoclusters. The other apparent characteristic of the doped two-cage nanochains is

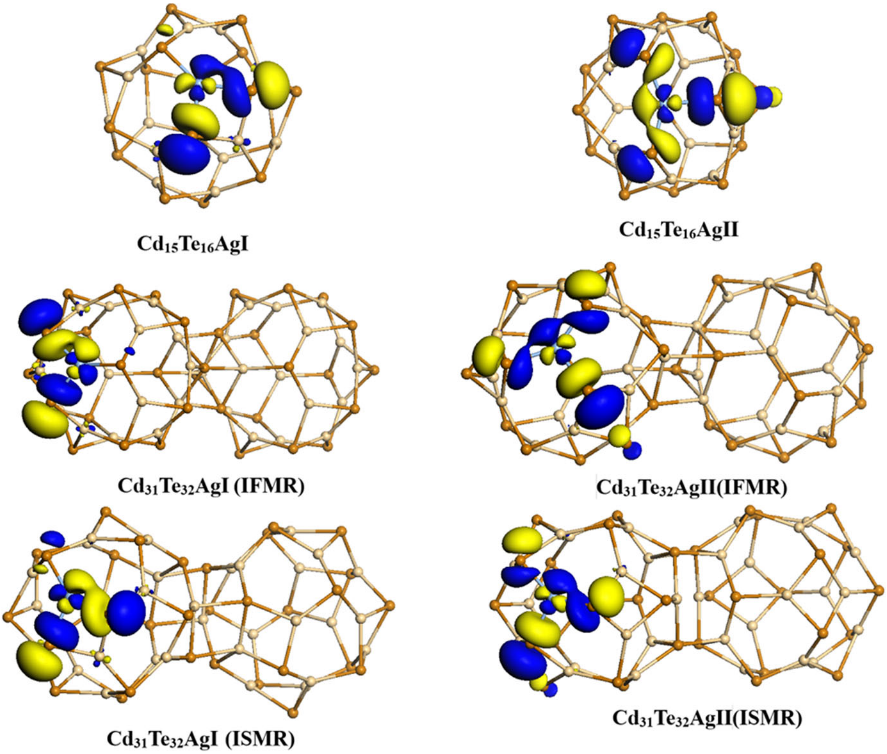

**$Cd_{15}Te_{16}AgI$** **$Cd_{15}Te_{16}AgII$**

**$Cd_{31}Te_{32}AgI$ (IFMR)** **$Cd_{31}Te_{32}AgII$(IFMR)**

**$Cd_{31}Te_{32}AgI$ (ISMR)** **$Cd_{31}Te_{32}AgII$(ISMR)**

**Fig. 7** The charge densities of the HOMO of $Cd_{15}Te_{16}Ag$ and $Cd_{31}Te_{32}Ag$ nanoclusters. The *dark brown*, *light brown* and *blue balls* represent Te, Cd, and Ag atoms respectively (Color figure online)

that the charge densities of HOMO-2 corresponding to the top of valence band are mainly dominated by the cage doped with Ag, which is different from the undoped two-cage nanochains as shown in Fig. 3. However, different doping sites do not show any significant effect on charge densities.

## Conclusion

In this paper, the structural and electronic properties of the undoped and doped $(CdTe)_{16}$ single cage and multi-cage nanochains ($N = 1$–3) are studied by density functional theory. $(CdTe)_{16}$ is chosen as the building unit to form multi-cage nanochains. Two possible assembly modes, interconnecting two $(CdTe)_{16}$ cages by two four-membered rings and interconnecting two $(CdTe)_{16}$ cages by two six-membered rings are considered. The study shows that multi-cage nanochains are more stable than the single cage. The $(CdTe)_{16\times N}$ IFMR nanochains have higher stability than that of ISMR nanochains with the same $N$. These results indicate that the stability is not only determined by the assembly number of cages but also relied on the assembly modes in $(CdTe)_{16\times N}$ nanochains. The energy gap of the nanochains, the energy difference between HOMO and LUMO, exhibits to vary with assembly modes and assembly number of cages. The $(CdTe)_{16\times N}$ ISMR nanochains have the narrower energy gaps comparing to the IFMR nanochains with the same $N$. In the analysis of the charge densities of LUMO and HOMO of $(CdTe)_{16\times N}$ nanochains, results show that the LUMO is composed of Cd $s$-orbital and Te $sp^3$ hybrid orbital, while the HOMO consists of major Te $p$-orbital and Cd $d$-orbital for both ISMR and IFMR nanochains. Additionally, the charge densities of LUMO and HOMO are mainly dominated by the middle atoms of nanochains.

In substitutionally doped single $Cd_{15}Te_{16}Ag$ cage and $Cd_{31}Te_{32}Ag$ two-cage nanochains, two substitutional sites, site I and site II, are discussed. The results show that the stability of Ag-doped nanoclusters is higher than that of corresponding undoped nanoclusters, indicating that Ag doping improves the stability of $(CdTe)_{16\times N}$ multi-cage nanoclusters. Besides, doped $(CdTe)_{16\times N}$ nanoclusters with Ag at doping site I are more stable than the doped nanoclusters with Ag at doping site II for the same assembly mode and $N$. So, both doping and doping site have influences on the stable of nanoclusters. Due to the Ag doping, an acceptor level $E_a$ is observed in the energy band gap. The charge density analysis shows that the contributions to the acceptor level mainly comes from the Ag-$d$ orbital and Te-$p$ orbital, which is consistent with the valence configurations of Ag and Te atoms. The charge densities of LUMO and HOMO-2 are mainly composed of Cd $s$-, Te-$sp^3$ hybrid orbitals and Te-$p$, Cd-$d$ orbitals showing the same characters as the LUMO and HOMO of undoped nanoclusters. In contrast to the undoped two-cage nanochains, the charge densities of the top of the valence band of doped two-cage nanochains are mainly dominated by the cage doped with Ag. All above results reveal that the structural and electronic properties of the multi-cage nanochains are strongly dependent on the assembly number of cages, assembly mode, doping and doping site in a nanochain.

**Acknowledgements** This work was supported by the National Natural Science Foundation of China (21376013). This paper is supported by "Chemical Grid Project" of Beijing University of Chemical Technology.

## References

1. S. K. Bhattacharya and A. Kshirsagar (2011). *Eur. Phys. J. D* **61**, 609.
2. L. E. Brus (1984). *J. Chem. Phys.* **80**, 4403.
3. X. Shen, J. Jia, Y. Lin, and X. Zhou (2015). *J. Power Sources* **277**, 215.
4. A. D. Stiff-Roberts, K. R. Lantz, and R. Pate (2009). *J. Phys. D Appl. Phys.* **42**, 234004.
5. J. Du, C. Wang, X. Xu, Z. Wang, S. Xu, and Y. Cui (2016). *Luminescence* **31**, 419.
6. J. Chen, A. Xiao, Z. Zhang, et al. (2015). *Spectrochim. Acta A* **151**, 506.
7. L. Ma, J. Wang, and G. Wang (2012). *Chem. Phys. Lett.* **552**, 73.
8. J. Wang, L. Ma, J. Zhao, and K. A. Jackson (2009). *J. Chem. Phys.* **130**, 214307.
9. Z. Wu, Y. Zhang, S. Huang, and S. Zhang (2013). *Comput. Mater. Sci.* **68**, 238.
10. R. Peköz and S. Erkoç (2009). *Comput. Mater. Sci.* **45**, 912.
11. S. Sriram and R. Chandiramouli (2015). *Res. Chem. Intermed.* **41**, 2095.
12. S. K. Bhattacharya and A. Kshirsagar (2007). *Phys. Rev. B* **75**, 035402.

13. M. Cargnello, et al. (2015). *Nature* **524**, 450.
14. D. J. Norris, A. L. Efros, and S. C. Erwin (2008). *Science* **3195871**, 1776.
15. Z. Rak, S. D. Mahanti, K. C. Mandal, and N. C. Fernelius (2009). *J. Phys. Chem. Solids* **70**, 344.
16. S. Xu, et al. (2014). *J. Mol. Model.* **20**, 2184.
17. X. D. Liu and T. Xing (2014). *Solid State Commun.* **187**, 72.
18. R. Car and M. Parrinello (1985). *Phys. Rev. Lett.* **55**, 2471.
19. R. O. Jones (2015). *Rev. Mod. Phys.* **87**, 897.
20. B. Delley (2000). *J. Chem. Phys.* **113**, 7756.
21. J. P. Perdew, K. Burke, and Y. Wang (1996). *Phys. Rev. B* **54**, 16533.
22. B. Hammer, L. B. Hansen, and J. K. Norskov (1999). *Phys. Rev. B* **59**, 7413.
23. X. Peng, et al. (2000). *Nature* **404**, 59.